
Journal of Computer-Aided Materials Design, **10:** 143–154, 2003.
KLUWER/ESCOM

Crack-tip dislocation nanostructures in dynamical fracture of fcc metals: A molecular dynamics study

HAJIME KIMIZUKA[a,*], HIDEO KABURAKI[b], FUTOSHI SHIMIZU[b] and JU LI[c]
[a]*Energy & Environment Technology Group, Science Division, The Japan Research Institute, Limited, Tokyo, 102-0082, Japan;* [b]*Center for Promotion of Computational Science and Engineering, Japan Atomic Energy Research Institute, Tokyo, 110-0015, Japan;* [c]*Department of Materials Science and Engineering, Ohio State University, Columbus, Ohio 43210, USA*

Received 11 October 2003; Accepted 12 November 2003

Abstract. Dynamic behavior of dislocations near a crack tip in an fcc lattice, studied through parallel molecular dynamics (MD) simulation with visualization facilitated by newly developed software, reveals three-dimensional features of dislocation nucleation and subsequent entanglement. Results obtained for copper and aluminum show multiple emissions of dislocation loops from the crack tip and incipient evolution of plastic deformation during crack extension. $\langle 100 \rangle$ dislocations are found to be emitted in aluminum at zero temperature, which however are unstable and subsequently disassociate into bundles of $\frac{1}{2}\langle 110 \rangle$ dislocations.

Keywords: aluminum, AtomEye, copper, dislocation emission, ductile fracture, Parallel Molecular Dynamics Stencil

1. Introduction

The evolution of crack-tip microstructure is a complex and highly nonlinear phenomenon central to the understanding of strength and failure of materials. Of fundamental interest are dislocation processes in a crack-tip stress field and their role in controlling the brittle versus ductile behavior [1, 2, 3, 4, 5]. Traditionally, brittle-to-ductile transition in metals is believed to be governed by dislocation nucleation [6, 7], whereas in a covalent material such as Si it is thought to be controlled by dislocation mobility [8, 9]. Despite the many attempts to elucidate the fundamental nature of crack-tip plasticity, our knowledge of the mechanistic details at the atomic level is meager because of limited resolution of experiments, and the limited ability of computer simulation to probe sufficiently long time and length scales.

In this paper, we report molecular dynamics (MD) results on the formation of dislocation nanostructures in face-centered-cubic (fcc) metals where two features are introduced. One is an MD code for parallel computing [10] and the other is a graphics software for visualization [11]. With these tools we carry out a study of the crack-tip responses to mode I loading in Cu and Al using optimized many-body interatomic potentials [12, 13]. We find that the crack tip initially extends in a cleavage manner in Cu at essentially zero temperature, but soon after, plastic deformation in the form of tip roughening sets in. Given this result it is perhaps not surprising that at 50 K roughening is observed with no delay. In contrast dislocation nucleation is observed in Al at all temperatures. Visualization of the interactions among the emitted dislocations reveals a complex scenario of loop expansion and break-up, along with

*To whom correspondence should be addressed. E-mail: kimizuka.hajime@jri.co.jp

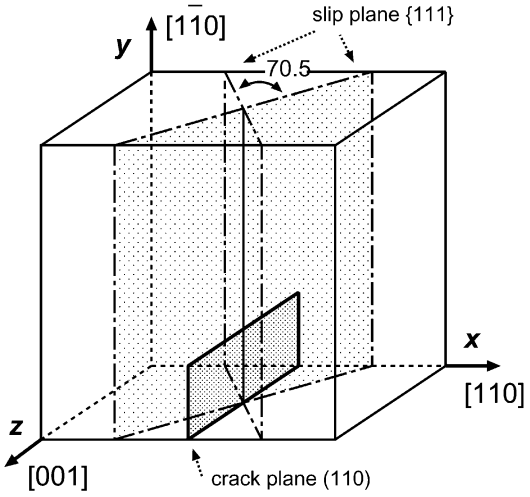

Figure 1. Simulation cell setup. The crack plane is on (110) and the crack front is along [001].

junction formation and unzipping behavior, which is somewhat reminiscent of the development of dislocation nanostructure observed in MD simulations of dislocation punch-out in nanoindentation [15, 16, 17, 18].

2. Computational method

2.1. Initial configuration

We use a $57\sqrt{2}a_0 \times 57\sqrt{2}a_0 \times 40a_0$ supercell (a_0 is the 0 K lattice constant), which contains approximately 1.04 million atoms. The atoms are initially put on a perfect fcc crystal lattice, with the crystallographic orientations shown in Fig. 1, where the x, y and z directions are [110], [1$\bar{1}$0] and [001], respectively. A crack is created initially to lie on the yz plane under an imposed overall uniaxial strain in the x direction. The initial crack length is $8.5\sqrt{2}a_0$ ($\simeq 0.15$ L_y) and the width is $\sqrt{2}a_0$. The crack plane and two relevant {111} slip planes are shown in Fig. 1. The setup is such that the (110) crack plane and the {111} slip planes intersect obliquely at an angle of 35.25° ($= 70.5° \times \frac{1}{2}$); neither of the {111} slip planes contain the [001] crack front. The dimensions of the Cu system are $291.5 \times 291.5 \times 144.6$ Å, with a crack length of 43.7 Å.

2.2. Molecular dynamics simulation of the fracture process

MD simulations are performed at finite temperatures in the microcanonical ensemble. The system is assigned a temperature ranging from 0 to 300 K by sampling the initial particle velocities from a Maxwellian distribution, after which it is equilibrated for over 2 ps by rescaling the velocities every 100 fs. The equation of motion is integrated using the velocity Verlet algorithm with a timestep of 2 fs. Tensile loading (mode I plane-strain) is applied in the x direction as follows. Atoms lying in the leftmost and rightmost (110) surfaces are constrained to move only on the yz plane. Displacement in x corresponding to a constant tensile strain rate of 2.32×10^9/s is imposed on the surface atoms at every timestep. Free boundary condition is applied in the y direction, whereas periodic boundary condition is applied in the z direction

(along the crack front). Total number of timesteps for all calculations are 16000, and the final strain at 32 ps is 0.0741. Under these conditions the crack is observed to expand laterally by ca. $4.2\sqrt{2}a_0$. All the MD simulations are performed in the *NVE* ensemble, without imposing temperature control during the deformation.

Embedded-atom (EAM) many-body interatomic potentials, developed by Mishin *et al.* [12, 13], are employed to simulate Cu and Al. The force-field parameters of these potentials are fitted to various experimental and *ab initio* data. The potentials include the fourth nearest neighbor shell interactions to accurately reproduce various structural, vibrational and mechanical properties, and to provide reliable energies for non-equilibrium structures. For comparison purposes, the Lennard-Jones (LJ) potential [14] is also used, with parameters $\epsilon = 0.167$ eV and $\sigma = 2.3151$ Å that gives $a_0 = 3.616$ Å in the case of Cu (with LJ potential, there is no distinction between Al and Cu besides rescaling). This LJ model potential has a smooth cut off between the fourth- and fifth-nearest neighbors at $1.49a_0$.

The simulations are performed using a modular and highly customizable MD code, the Parallel Molecular Dynamics Stencil (PMDS). The PMDS, developed by some of us, is a library of subroutines for carrying out large-scale MD simulations on a variety of parallel computing platforms. It is written in C language and MPI (message passing interface) for parallelization, and structured in such a way to conceal MPI functions from the top-level functions, so that the users are able to perform parallel simulations without any detailed knowledge of parallel programming. A typical main program consists of a chain of calls to PMDS functions. These functions correspond to modular parts of the MD algorithm and perform computing tasks in parallel automatically, such as distributing local atom data among other processors. With the help of PMDS, the users are able to build a parallel MD program effortlessly, just like using a 'stencil' in drawing.

The PMDS supports two major parallel decomposition algorithms for atomistic calculations, i.e. the spatial decomposition and the particle decomposition. Irrespective of which decomposition algorithm is adopted, the PMDS will generate Verlet neighbor lists for all the atoms in the same data structure, after the neighboring atoms of each atom are detected, listed, and distributed to the appropriate processor. Since the PMDS functions take care of the most tedious parts of a MD program, one can convert the PMDS code to the force field of one's interest if one only makes partial modifications associated with the interatomic potential. In most cases, this part can be written in a similar way as the serial code. The PMDS source codes are available on the World Wide Web [10]. For the present studies, the functions describing the boundary conditions are attached as an extra module to the original PMDS to simulate fracture of a notched solid.

2.3. Visualization of dislocation nanostructures

The atomic structures of defects near the crack-tip are visualized by two methods of discrimination, based on the potential energy and the coordination number, respectively. Only atoms in the defect cores are extracted from the large amount of atomic data generated from the MD simulations.

Fig. 2 shows the crack-tip dislocation nanostructures visualized using the two methods. With the potential energy discrimination, we plot only the atoms whose energies are slightly above the perfect fcc lattice cohesive energy. Choosing an appropriate value of the threshold energy allows us to extract the atoms lying in the core of the dislocations. In Fig. 2 (b), the threshold energies are varied from -342.1 to -336.1 kJ/mol. We observe that the disloca-

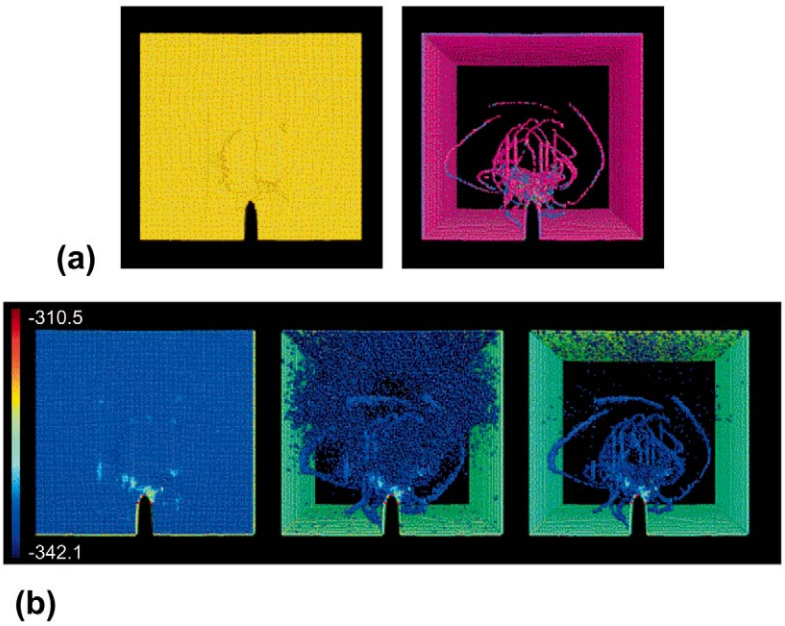

Figure 2. Crack-tip dislocation nanostructures, visualized by (a) coordination-number, and (b) potential-energy color encoding. The atoms whose coordination number equals to 10, 11 and 13 are represented as limegreen, mediumvioletred and royalblue spheres, respectively. In (b), the lower threshold energy is taken to be −342.1 (left), −337.5 (center) and −336.1 (right) kJ/mol, respectively.

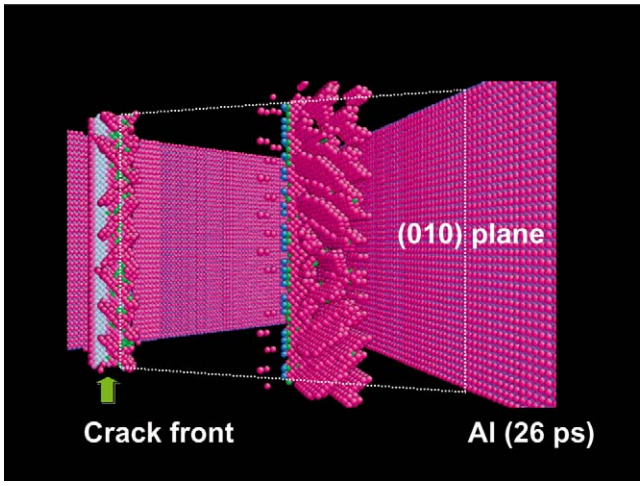

Figure 11. A ⟨100⟩ dislocation in Al crystal that is moving away from the crack tip (at 0 K). This dislocation is unstable and is in the process of breaking up, resulting in a temporarily wide and out-of-plane core.

tion nanostructures near the crack tip can be delineated more clearly as the threshold value increases. On the other hand, with the coordination number discrimination, the number of nearest-neighbor atoms is counted for each atom. In Fig. 2 (a), the atoms whose coordination number equals to 12 (perfect fcc/hcp structure) are rendered invisible. Note that the crack-tip nanostructures extracted by either method are very similar. However, the coordination number

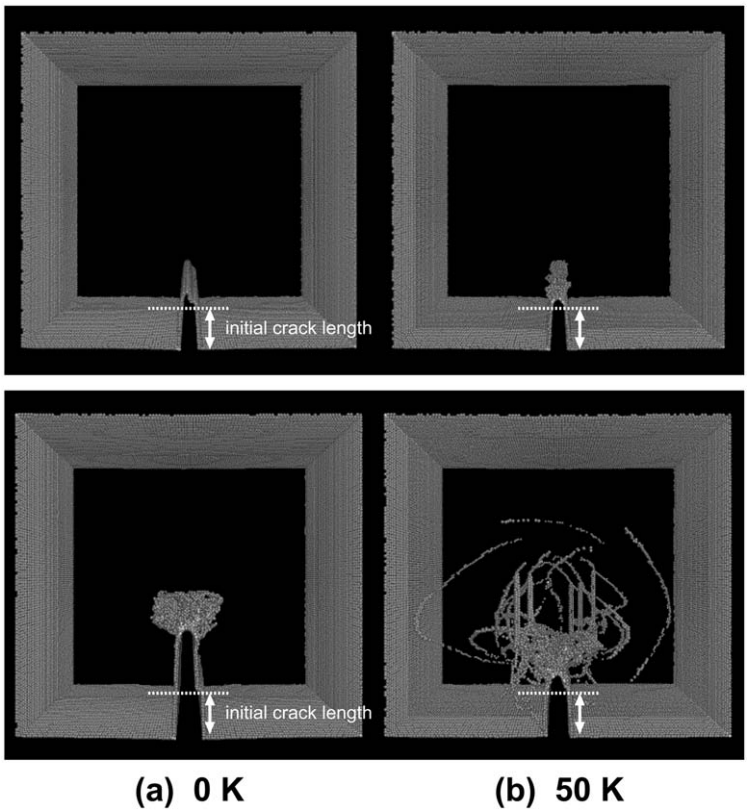

Figure 3. Crack-tip dislocation nanostructures in Cu at different temperatures ($t = 16$ ps in the upper two graphs and $t = 24$ ps in the lower two graphs).

discrimination is somewhat superior to the potential energy discrimination because the latter leads to noisy results when applied to dynamical configurations at finite temperatures.

The visualization software used in this study is a free atomistic configuration viewer, AtomEye [11]. It is based on a new graphics core library of higher drawing quality than the X-window standard, with area-weighted anti-aliasing. An order-N neighborlist algorithm is used to compute the bonding connectivity. The functionalities of AtomEye include: parallel and perspective projections with full three-dimensional navigation; customizable bond and coordination number calculation; color-encoding of arbitrary user-defined quantities; local atomic strain invariant color-encoding; colored atom tiling and tracing; up to 16 cutting planes; periodic boundary condition translations; high-quality JPEG, PNG and EPS screenshots; and animation scripting. The program is efficient compared to OpenGL® hardware acceleration by employing special algorithms to treat spheres (atoms) and cylinders (bonds), in which they are rendered as primitive objects rather than as composites of polygons. It can handle more than one million atoms on a PC with 1 GB memory. AtomEye is a robust, low-cost tool for surveying nanostructures and following their evolutions, and is available on all major UNIX platforms, Linux, Windows/Cygwin and Mac OS X/Darwin.

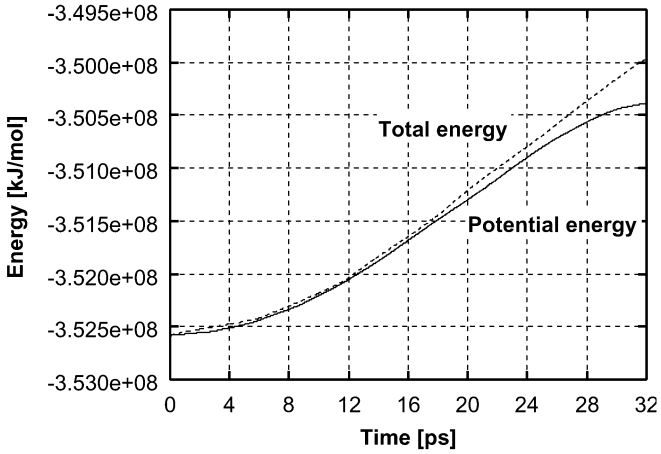

Figure 4. Time evolution of the total and potential energies of the Cu system during the fracture process (at 0 K).

3. Results and discussions

3.1. Plastic deformation processes in copper near the crack tip

During uniaxial loading, the atoms first readjust to the positions prescribed by linear elasticity theory, and then blunting occurs at the crack tip as multiple dislocations are emitted. In our simulations for the $(110)\langle 1\bar{1}0\rangle$ crack system of Cu, distinctly different behaviors are observed at ca. 0 K and at 50 K and above. In Fig. 3, snapshots are taken at 16 and 24 ps. For the 0 K system at 16 ps, the crack starts to extend in a brittle manner, as the nearest-neighbor bonds along the crack front are successively broken to form new (110) surfaces. As the applied strain increases, at 24 ps, the crack tip begins to roughen by emitting dislocations. In contrast, at 50 K, emission of dislocations from the crack tip can be observed during the early stage of loading and there is little sign of brittle fracture relative to the behavior at 0 K. Prolific dislocation nucleation and mobility leading to crack-tip blunting and arrest of the crack front are observed in all simulations at finite temperatures.

At 0 K, dislocation nucleation occurs only when the local stress exceeds a critical value, which is then followed by a sudden burst of dislocation activities. The transition from brittle crack propagation to crack-tip plasticity is sharp at 0 K. At finite temperatures, however, the energy barrier for dislocation nucleation can be overcome by thermal fluctuations; as a result, dislocation nucleation and plastic relaxation occur earlier and less abruptly than at 0 K, leading to a less concentrated dislocation 'cloud' than that of 0 K at $t = 24$ ps (Fig. 3). From 50 K to 300 K, we find little variation in the onset of dislocation activities with strain, as the resulting defect configurations have very similar appearances.

Fig. 4 and 5 plot the energy and average temperature of the system with time. In the *NVE*-ensemble simulation with moving atomistic walls, the total energy of the system continuously increases due to the external work done to the system, accompanied by growth of the potential energy. At 16 ps, when crack extension and/or dislocation emission at the crack tip occur, the potential energy shows deviation from the total energy, indicating inelastic deformation and dissipation. The average temperature of the system, derived from the kinetic energies of the atoms, is seen to maintain its initial value during the loading until ca. 16 ps, at which point it starts to increase as the emitted dislocations begin to glide across the system.

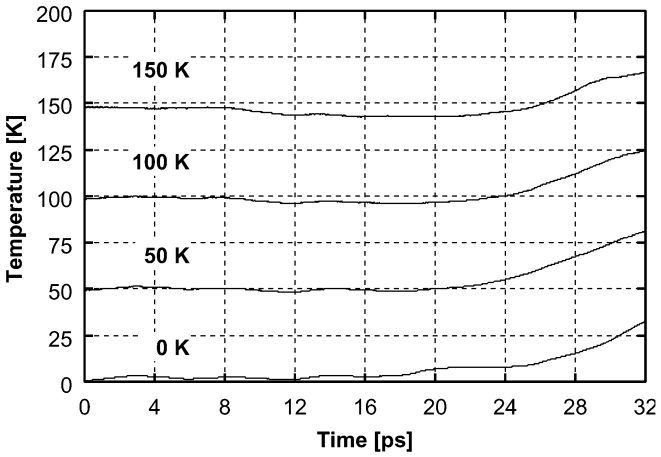

Figure 5. Time evolution of the average temperatures of the Cu system during the fracture processes.

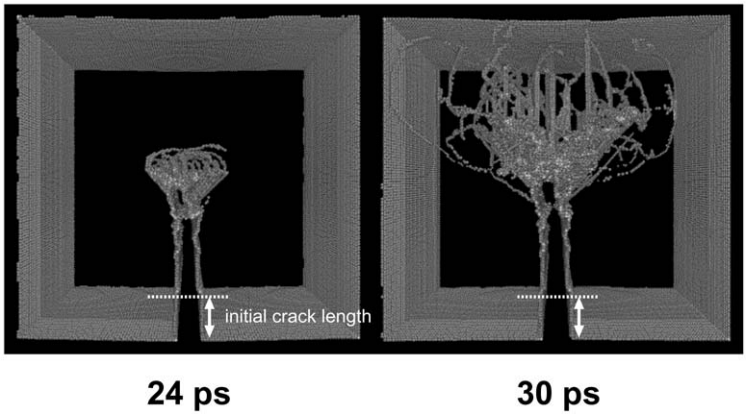

Figure 6. Snapshots of the crack-tip dislocation nanostructures in LJ-model crystal (at 0 K).

It is interesting to note that similar dynamical brittle-to-ductile transition behavior is observed in LJ-model crystal at 0 K as well (Fig. 6). In the LJ-model Cu, the crack front extends more readily in a cleavage manner compared to the EAM Cu. But soon after, similar plastic relaxations begin in the form of tip roughening. Because the stacking fault energy of fcc solid interacting via the LJ potential is low, the equilibrium width of the stacking-fault ribbons between the two partials is $\sim 9.6a_0$ [19], whereas the width in the actual [20] (and EAM-model [13]) Cu crystals is confined to $\sim 5a_0$. Although the LJ potential is considered to be unsuitable for describing the defect structures in fcc metals, the resulting defect configurations have rather similar appearances with EAM. It suggests that, in the early stage of crack-tip plasticity in Cu, the intrinsic stacking-fault energy does not have significant effect on the formation of dislocation nanostructures.

3.2. Dislocation motion on the glide planes in copper

Fig. 7 shows three-dimensional views of the evolution of dislocation nanostructures near the crack at 50 K. We observe multiple dislocation emissions at the crack tip, and the continuous expansion of a number of dislocation loops as time progresses. On one {111} slip plane, we can see a fan-shaped dislocation loop expanding steadily in a self-similar manner (Fig. 8).

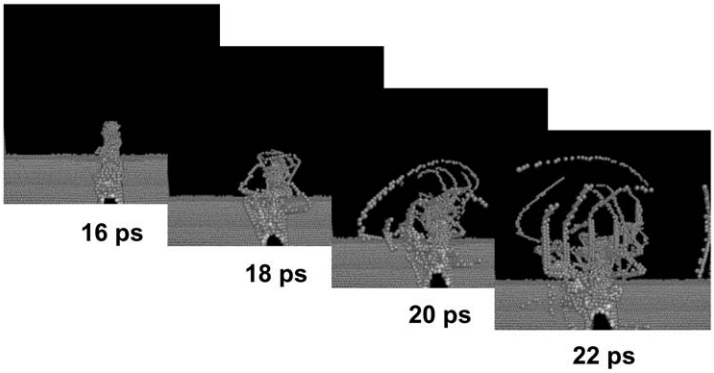

Figure 7. Three-dimensional views of the dislocation nanostructure in Cu crystal in the vicinity of the crack tip (at 50 K).

This loop, the inside of which is faulted, consists of semicircular Shockley partial dislocation with straight partial segments on the two sides. The semicircular partial dislocation grows and moves away from the crack tip, while the two straight segments radiate from the crack tip. These straight partial dislocation segments are conjectured to run along the partition line at which the $\{111\}\langle 11\bar{2}\rangle$ resolved shear stress of the crack-tip stress field goes from positive to negative, so the $\frac{1}{6}\langle 11\bar{2}\rangle$ partial dislocation has no incentive to expand further.

As time goes on, different dislocation loops intersect. Then the motion of a loop is arrested, and a stair-rod dislocation is formed inside the loop as shown in Fig. 8. However, upon further increased loading, we see a dislocation loop overcoming the barrier of a stair-rod dislocation, and starting to expand again. We also see that some stair-rod dislocations are unzipped later with the help of other dislocations.

3.3. Dislocation processes in aluminum

MD results of the dislocation emission processes near the crack tip of Cu and Al crystals at zero temperature are shown in Fig. 9 and 10, respectively. While a sharp crack advances in Cu under an applied load at 22 ps, in the case of Al two dislocations parallel to the crack front on the $\{010\}$ planes (at $\theta = 45°$) are emitted from the crack tip into the bulk. They glide in the $\langle 100\rangle$ directions, but gradually lose their shape and disintegrate into two bundles of $\frac{1}{2}\langle 110\rangle$ dislocations on different slip planes. Profuse generations of $\frac{1}{2}\langle 110\rangle$ dislocations on the easier $\{111\}$ slip planes subsequently occur in the vicinity of the initially-emitted $\langle 100\rangle$ dislocations and the crack-tip as well (Fig. 11).

In fcc crystals, the shortest lattice vectors which are the most likely dislocation Burgers vectors, are of the type $\frac{1}{2}\langle 110\rangle$ and $\langle 100\rangle$. In an elastically isotropic medium (which is a good approximation for Al), the elastic energy of a dislocation is proportional to the square of its Burgers vector, so the energy of a $\frac{1}{2}\langle 110\rangle$ dislocation is only half of that of $\langle 001\rangle$. Thus, the $\langle 100\rangle$ dislocations are much less favorable energetically and, in fact, are only rarely observed [20]. We find that the initially-emitted $\langle 100\rangle$ dislocations cannot hold their shape and disintegrate into many $\frac{1}{2}\langle 110\rangle$ dislocations on the easier slip planes. This phenomenon is in accordance with the above energy discussion.

Fig. 12 shows the sectional snapshots of the emission of $\langle 100\rangle$ dislocation on the (010) plane. In general, the nucleation of a dislocation at the crack tip necessarily involves the formation of a surface defect (an extrinsic step) resulting from the sliding on a glide plane. At

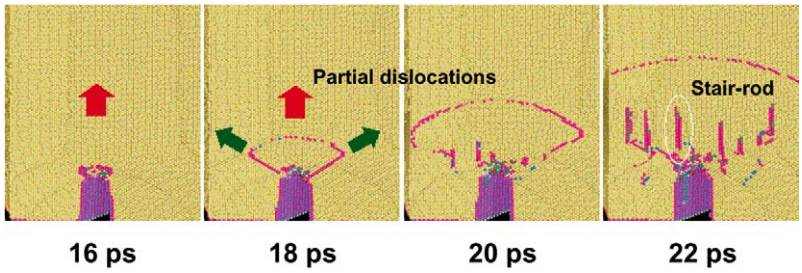

Figure 8. Snapshots of fan-like dislocation loop expansion on the slip plane in Cu crystal (at 50 K).

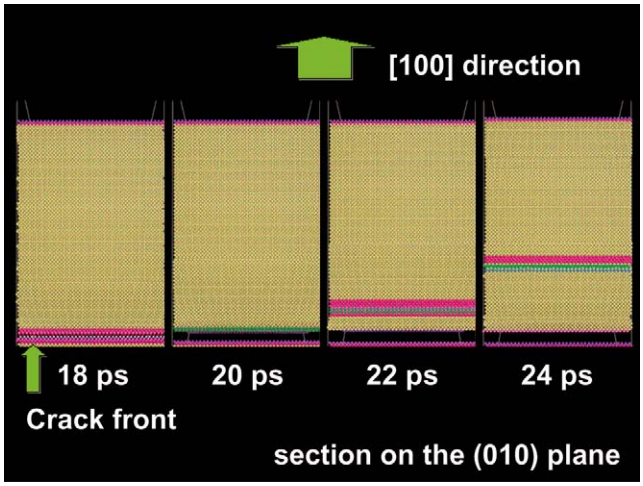

Figure 12. Snapshots of the glide motion of a ⟨100⟩ dislocation on the {010} plane (at 0 K), moving away from the crack tip.

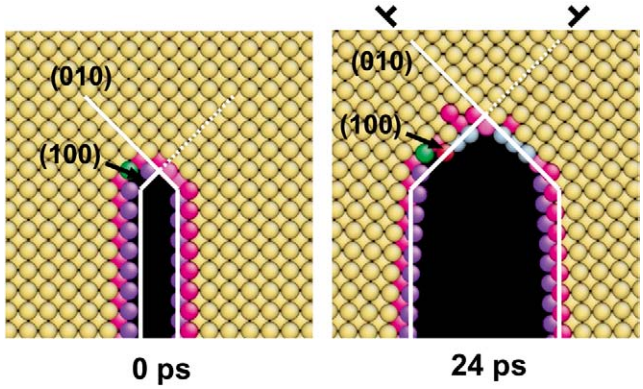

Figure 13. After nucleation of two ⟨100⟩ dislocations from the {010} surfaces vicinal to the crack plane, steps are formed on the crack tip that blunt it.

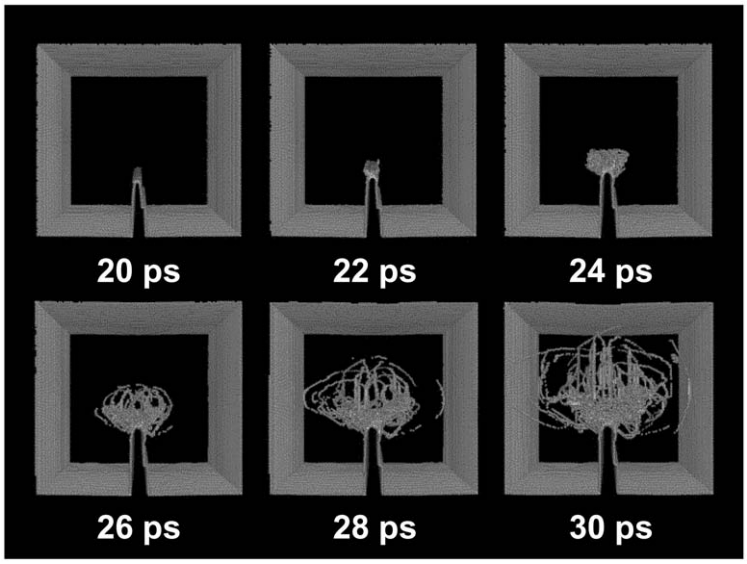

Figure 9. MD simulation of dislocation emission near the crack tip of Cu crystal (at 0 K).

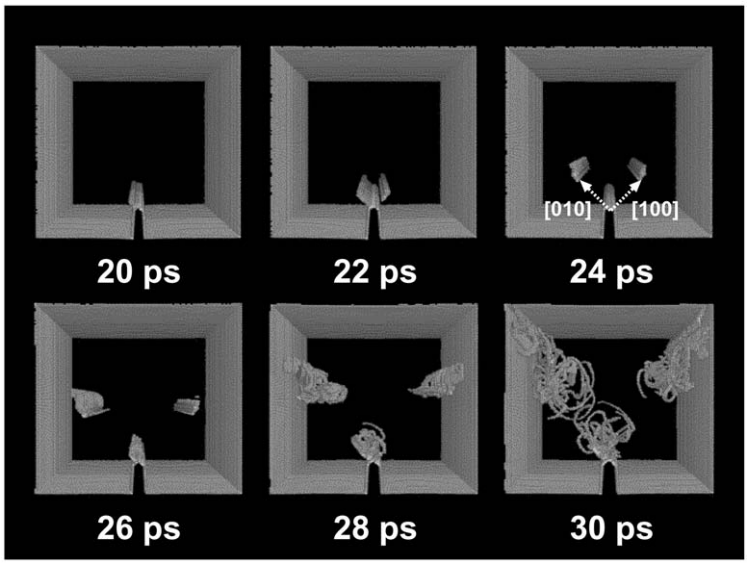

Figure 10. MD simulation of dislocation emission near the crack tip of Al crystal (at 0 K). Two dislocations of $\langle 100 \rangle$ character are emitted first and move away from the crack tip ($t = 24$ and 26 ps), which eventually disintegrate into two bundles of $\frac{1}{2}\langle 110 \rangle$ dislocations ($t = 28$ and 30 ps).

20 ps, nearest-neighbor bonds break at the crack front and two blocks of crystal begin to slide about a particular (010) plane, and thus defects are nucleated at the crack tip, consisting of an extrinsic step/dislocation pair. Soon after, it can be seen that the dislocation core glides along the $\langle 100 \rangle$ direction on the (010) plane into the bulk. The products of the nucleation process consist of a stable extrinsic surface step and a fully-formed dislocation core separated from the crack tip. This process of rearranging the atom stacking planes leads to the blunting of the crack tip as seen in Fig. 13.

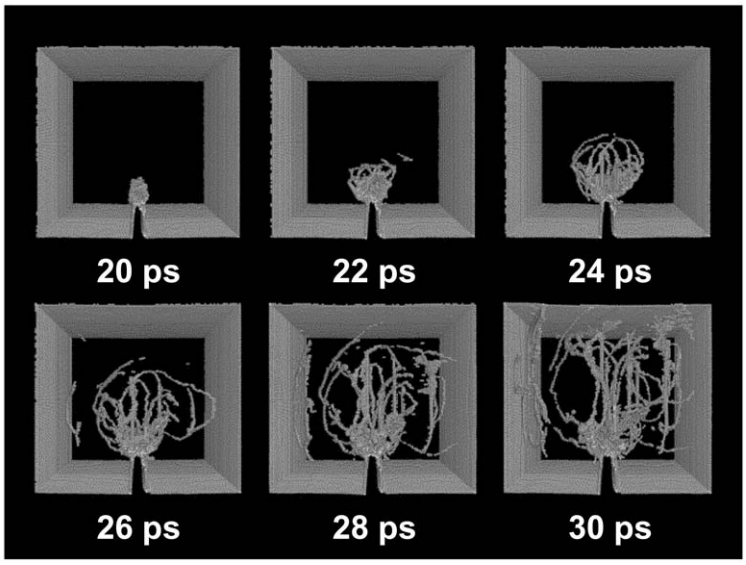

Figure 14. Dislocation emission processes near the crack tip of Al crystal (at 50 K).

The ⟨100⟩ dislocation emission process is not observed in Cu. In the early stage of deformation in Cu, a sharp crack advances first, and the local crystal symmetry near the crack tip becomes reduced significantly, before a dislocation is clearly emitted from the crack tip and an extrinsic step is formed. Even in Al, at finite temperatures the conventional $\frac{1}{2}\langle 110\rangle$ dislocation emission is dominant and the ⟨100⟩ dislocations are not observed (Fig. 14).

4. Summary

Classical molecular dynamics simulations with a million atoms are carried out to study the effect of temperature on the fracture processes of Cu and Al. We show that the MD method combined with visualization is well suited for gaining mechanistic insights into the dynamical failure processes at finite temperatures. The simulations reveal that crack extension in Cu at zero temperature occurs in a brittle manner at first, and then the crack tip begins to roughen through profuse dislocation emissions. Crack-tip blunting by dislocation nucleation eventually arrests crack propagation. In Al at a starting temperature of 0 K, we find that dislocations of ⟨100⟩ character are nucleated first on the {010} planes, propagate away from the crack tip, and then break up into bundles of $\frac{1}{2}\langle 110\rangle$ dislocation loops on oblique {111} slip planes. The differences in the behaviors of Al and Cu might be attributed to their different degrees of elastic anisotropy [15, 16, 17], the abnormally large intrinsic stacking fault of Al and directional bonding in Al [21].

Acknowledgements

We thank Sidney Yip for support and encouragements during the research and writing of this manuscript. We thank Riichiro Okawa and Tomoko Kadoyoshi for numerous discussions on the application of PMDS and AtomEye to the large-scale defect simulations and their effort in testing the programs. This study was supported by 'Research and Development for Applying Advanced Computational Science and Technology' of Japan Science and Technology

Corporation (ACT-JST, No. 13A-4). JL acknowledges support by Honda R&D Co., Ltd. (RF# 744252) and the OSU Transportation Research Endowment Program.

References

1. Cleri, F., Yip, S., Wolf, D. and Phillpot, S.R., Atomic-scale mechanism of crack-tip plasticity: dislocation nucleation and crack-tip shielding, Phys. Rev. Lett., 79 (1997) 1309.
2. Abraham, F.F., Schneider, D., Land, B., Lifka, D., Skovira, J., Gerner, J. and Rosenkrantz, M., Instability dynamics in three-dimensional fracture: an atomistic simulation, J. Mech. Phys. Solids, 45 (1997) 1461.
3. Bulatov, V., Abraham, F.F., Kubin, L., Devincre, B. and Yip, S., Connecting atomistic and mesoscale simulations of crystal plasticity, Nature, 391 (1998) 669.
4. Farkas, D., Duranduru, M., Curtin, W.A. and Ribbens, C., Multiple-dislocation emission from the crack tip in the ductile fracture of Al, Phil. Mag., A 81 (2001) 1241.
5. Abraham, F.F., Walkup, R., Gao, H.J., Duchaineau, M., de la Rubia, T.D. and Seager, M., Simulating materials failure by using up to one billion atoms and the world's fastest computer: Work-hardening, Proc. Natl. Acad. Sci. USA, 99 (2002) 5783.
6. Rice, J.R. and Thomson, R., Ductile versus brittle behaviour of crystals, Phil. Mag., 29 (1974) 73.
7. Rice, J.R., Dislocation nucleation from a crack tip: an analysis based on the Peierls concept, J. Mech. Phys. Solids, 40 (1992) 239.
8. Gumbsch, P., Riedle, J., Hartmaier, A. and Fischmeister, H.F., Controlling Factors for the Brittle-to-Ductile Transition in Tungsten Single Crystals, Science, 282 (1998) 1293.
9. Argon, A.S. and Gally, B.J., Selection of crack-tip slip systems in the thermal arrest of cleavage cracks in dislocation-free silicon single crystals, Scripta Mater., 45 (2001) 1287.
10. The source programs (written in C language and MPI) are available on the WWW at http://stencil.koma.jaeri.go.jp/.
11. Li, J., AtomEye: an efficient atomistic configuration viewer, Modelling Simul. Mater. Sci. Eng. 11 (2003) 173. The binaries for various platforms are available on the WWW at http://alum.mit.edu/www/liju99/Graphics/A/.
12. Mishin, Y., Farkas, D., Mehl, M.J. and Papaconstantopoulos, D.A., Interatomic potentials for monoatomic metals from experimental data and ab initio calculations, Phys. Rev., B 59 (1999) 3393.
13. Mishin, Y., Mehl, M.J., Papaconstantopoulos, D.A., Voter, A.F. and Kress, J.D., Structural stability and lattice defects in copper: Ab initio, tight-binding and embedded-atom calculations, Phys. Rev., B 63 (2001) 224106.
14. Kluge, M.D., Wolf, D., Lutsko, J.F. and Phillpot, S.R., Formalism for the calculation of local elastic constants at grain boundaries by means of atomistic simulation, J. Appl. Phys., 67 (1990) 2370.
15. Li, J., Van Vliet, K.J., Zhu, T., Yip, S. and Suresh, S., Atomistic mechanisms governing elastic limit and incipient plasticity in crystals, Nature, 418 (2002) 307.
16. Van Vliet, K.J., Li, J., Zhu, T., Yip, S. and Suresh, S., Quantifying the early stages of plasticity through nanoscale experiments and simulations, Phys. Rev., B 67 (2003) 104105.
17. Zhu, T., Li, J., Van Vliet, K.J., Ogata, S. Yip, S. and Suresh, S., Predicative Modeling of Nanoindentation Induced Dislocation Nucleation in Copper, J. Mech. Phys. Solids, (2003), in print.
18. Choi, Y., Van Vliet, K.J., Li, J. and Suresh, S., Size effects on the onset of plastic deformation during nanoindentation of thin films and patterned lines, J. Appl. Phys., 94 (2003) 6050.
19. Kogure, Y., Tsuchiya, T. and Hiki, Y., Simulation of dislocation configuration in rare gas crystals, J. Phys. Soc. Jpn., 56 (1987) 989.
20. Hull, D. and Bacon, D.J., Introduction to Dislocations, 4th ed. (Butterworth-Heinemann, Oxford, 2001).
21. Ogata, S., Li, J. and Yip, S., Ideal pure shear strength of aluminum and copper, Science, 298 (2002) 807.